Mat. Res. Soc. Symp. Proc. Vol. 658 © 2001 Materials Research Society

Micromagnetic and Magnetoresistance Studies of Ferromagnetic $La_{0.83}Sr_{0.13}MnO_{2.98}$ Crystals

Guerman Popov,[a] Sergei V. Kalinin,[b] Rodolfo A. Alvarez,[b] Martha Greenblatt,[a] and Dawn A. Bonnell [b]

[a] Department of Chemistry, Rutgers, the State University of New Jersey, Piscataway, New Jersey 08854, USA

[b] Department of Materials Science and Engineering, University of Pennsylvania, Philadelphia, Pennsylvania, 19104, USA

ABSTRACT

Magnetic force microscopy (MFM) and atomic force microscopy (AFM) were used to investigate the surface topography and micromagnetic structure of $La_{0.83}Sr_{0.13}MnO_{2.98}$ single crystals with colossal magnetoresistance (CMR). The crystals were grown by fused salt electrolysis and characterized by chemical analysis, X-ray diffraction, magnetic and transport measurements. The crystals are rhombohedral ($R\bar{3}c$). Magnetic and transport measurements indicate that the ferromagnetic ordering at 310 K is associated with an insulator-metal transition at the same temperature. A maximum negative magnetoresistance (-62 %) is observed at 290 K in an applied magnetic field of 5 T. The magnetoresistance increases in magnitude sharply (1.8 %), comparing to the rest of the change, with increasing magnetic field up to 20 G, and then it increases slowly with increasing field.

MFM and AFM were used to study the (110) surface as well as a number of unspecified surfaces. Surface topography of an as-grown crystal exhibits well-developed surface corrugations due to extensive twinning. The corrugation angle at twin boundaries can be related to the unit cell parameters, surface and twinning planes. Magnetic force microscopy images show that magnetic domain boundaries are pinned to the crystallographic twins; a small number of unpinned boundaries are observed. The statistical analysis of domain boundary angle distribution is consistent with cubic magnetocrystalline anisotropy with easy axis along [100] directions for this material. Unusual magnetization behavior in the vicinity of topological defects on the surface is also reported. MFM contrast was found to disappear above the ferromagnetic Curie temperature; after cooling a new magnetic structure comprised of Bloch walls of opposite chiralities developed.

INTRODUCTION

$LnMnO_3$-type rare earth manganates have received recent interest, because of the discovery of colossal magnetoresistance (CMR), the effect by which the electrical resistivity decreases by orders of magnitude upon the application of a magnetic field. CMR properties of polycrystalline materials and thin films have been studied extensively. It was shown that CMR behavior in many cases is associated with magnetic disorder at grain and domain boundaries [1]. Hence, the origins of CMR behavior of these materials can be best understood from the combination of spatially resolved local and single crystal studies.

$La_{1-x}Sr_xMnO_3$ is a typical perovskite CMR system [2-7]. Its structural symmetry changes from orthorhombic to rhombohedral with increasing *x* up to 0.8. Depending on *x* in

$La_{1-x}Sr_xMnO_3$ and oxygen stoichiometry the ferromagnetic transition may vary greatly [2, 7]. Compositions with T_c above room temperature can be obtained.

In this work we undertake micromagnetic studies on $La_{0.83}Sr_{0.13}MnO_{2.98}$ single crystals. While many single crystal growth techniques require special equipment and are in general difficult to utilize, recently the fused salt electrolysis technique was proven to be an easy method of growing single crystals of doped rare earth manganates [2].

EXPERIMENTAL

The synthesis conditions were similar to those described in [2]. The crystals of $La_{0.83}Sr_{0.13}MnO_{2.98}$ were grown by electrolysis in a melt obtained from a mixture of Cs_2MoO_4 and MoO_3 to which $SrMoO_4$, $MnCO_3$ and La_2O_3 were added. The molar ratios were 2.00 : 1.00 : 0.390 : 0.740 : 0.280 respectively. Electrolysis was carried out in an yttria-stabilized zirconia crucible using Pt electrodes, in air, at 975°C for 73 hours using an 18 mA current. Electrolysis was terminated by lifting the electrodes from the melt. The use of a zirconia crucible and not alumina was necessary to prevent incorporation of aluminum that can be abstracted from the crucible [8]. The anode product was washed in a warm solution of 5 % K_2CO_3 and 2.5 % disodium ethylenediaminetetraacetate.

Chemical analyses for La, Sr and Mn were carried out with a Baird Atomic Model 2070 inductively coupled plasma emission spectrometer (ICP). The sample was quantitatively dissolved in HCl. The solution was diluted appropriately to bring the concentrations of the studied elements within the range of the available standards. Analyses are accurate to within 1-2 %. The formal average oxidation state of manganese was established by iodometric titration employing an amperometric dead-stop end point method [9]. Lattice parameters were determined by Rietveld refinement employing the GSAS software package [10]. Data for Rietveld refinement was collected on finely ground crystals using a Scintag PAD V diffractometer (CuK_α radiation) in the range $2\theta = 10° – 120°$.

The index of the face used in MFM study was determined with a CAD4 diffractometer using graphite monochromatized Mo K_α radiation (λ = 0.71073 Å). Electrical resistivity measurements were made by a four-probe technique. Magnetic and magnetoresistance measurements were performed on a piece containing intergrown crystals in a Quantum Design SQUID magnetometer (MPMS) between 4 K and 400 K.

The AFM and MFM measurements were performed on a commercial instrument (Digital Instruments Dimension 3000 NS-III). Unpoled CoCr coated Magnetic Force Etched Silicon Probe (MESP) tips ($l \approx$ 225 μm, resonant frequency ~60 kHz, $k \approx$ 1-5 N/m) were used. The lift height for the interleave scans in the MFM was usually 100 nm. The scan rate varied from 0.2 Hz for large scans (~60 μm) to 1 Hz for smaller scans (~10 μm). The low coercive field of the CMR samples used precluded imaging at lower lift heights and application of strongly magnetized tips.

RESULTS AND DISCUSSION

The product crystals grow directly on the anode in the form of batches of black intergrown highly reflecting crystals with cubic-like habits. The dimensions of the individual crystallites were typically 0.5– 1.5 mm on an edge. The average manganese oxidation state was found

to be +3.213. Based on the results of ICP and titration, the composition of the sample is $La_{0.83}Sr_{0.13}MnO_{2.98}$.

The powder X-ray diffraction pattern was indexed in rhombohedral symmetry. No evidence of non-uniform composition of the solid solution $La_{1-x}Sr_xMnO_{3-\delta}$, such as unusual broadening or doubling of peaks, was found. The lattice parameters of the studied crystals are a = 5.4805(4) Å and α = 60.602(1)° in the rhombohedral setting. The lattice parameters in rhombohedral setting indicate that the structure is only slightly distorted from cubic symmetry ($\alpha \approx 60°$). Figure 1a shows the temperature dependence of magnetization at an applied field of 100 G and the temperature dependence of resistivity at zero field, as well as the magnetoresistance at 5 T. Magnetoresistance (MR%) is defined as $[(\rho(5T)- \rho(0))/\rho(0)]\times100$, where ρ(0) and ρ(5T) are the resistivities at an applied field of zero and 5 Tesla respectively. The sample shows typical behavior for the hole-doped manganese perovskites. The ferromagnetic ordering is accompanied by an insulator-metal transition at 310 K. $T_{c,\ onset}$ of the ordering is 334 K and it is complete at 280 K. Maximum magnetoresistance, –62 %, is observed at 290 K and 5 T (Figure 1a).

Figure 1b presents the hysteresis measurements taken at 293 K. The coercive field of this sample is 21 G, however, saturation is not fully achieved even at an applied field of 5 T. Figure 1c shows the dependence of magnetoresistance on the magnetic field at 300 K. The negative magnetoresistance increases in magnitude with increasing magnetic field, however, there is a

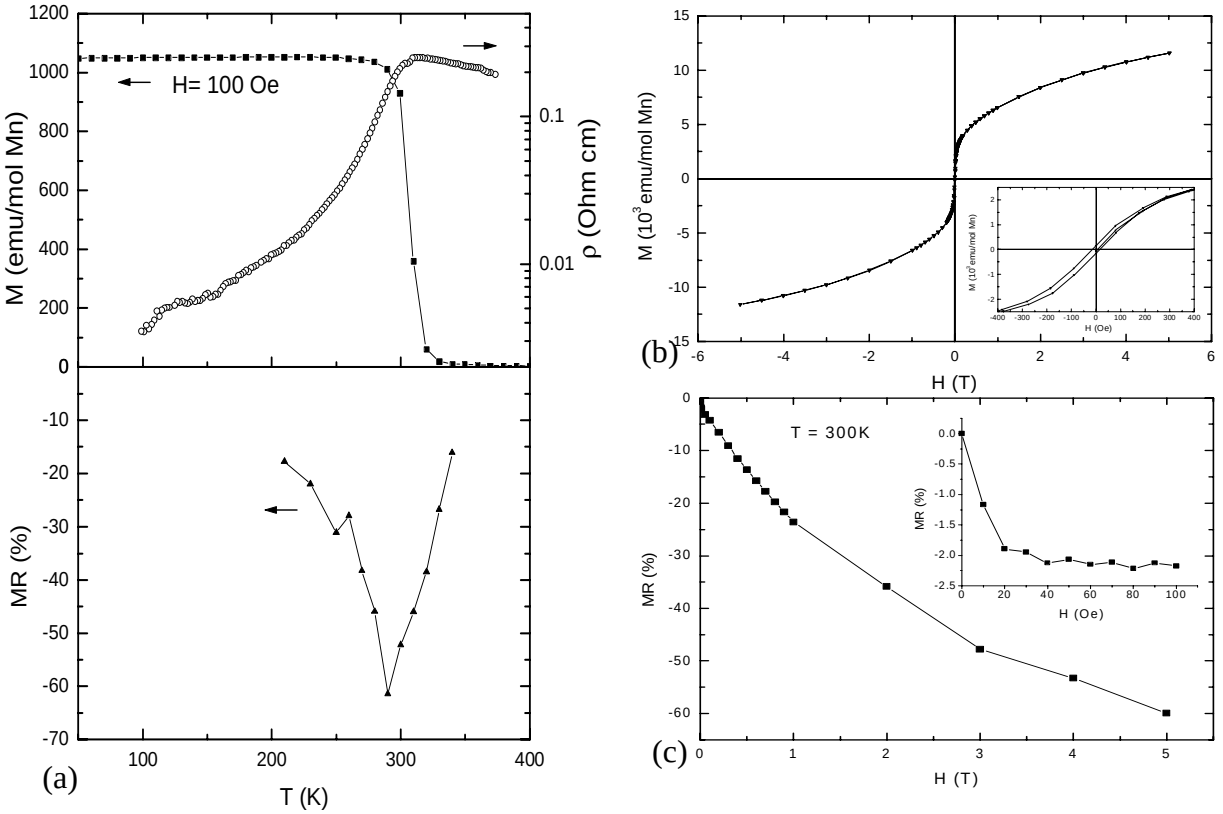

Figure 1. *(a) Temperature dependent magnetization, resistivity, magnetoresistance, (b) hysteresis, and (c) field dependence of magnetoresistance of* $La_{0.83}Sr_{0.13}MnO_{2.98}$.

sharp negative magnetoresistance change at low field of ~20 G (see Figure 1c inset). Taking into consideration the coercive field value of 21 G we conclude that this sharp change in MR is attributed to magnetic domain reorientation.

The magnetic parameters of $La_{0.83}Sr_{0.13}MnO_{2.98}$ were derived by fitting the magnetic susceptibility in the paramagnetic range to the Curie-Weiss law ($\chi = C/(T-\theta)$). The effective magnetic moment was found to be $\mu_{eff} = 5.61\ \mu_B$ and $\theta = 308$ K. From the data of the average manganese oxidation state, the calculated spin-only magnetic moment is $\mu_{calc} = 4.70\ \mu_B$. The experimental value of the magnetic moment is larger than expected (μ_{calc}), which can be attributed to the formation of superparamagnetic clusters [11].

The surface topography and the magnetic structure of the crystals were studied by various scanning probe microscopy (SPM) techniques [12]. The presence of crystallographic twin boundaries results in formation of surface corrugations on the topographical image (Figure 2). The images indicate a high degree of twinning with characteristic twin sizes of 5-20 μm, which is expected for this type of material [3]. The corrugation angles for the twins were $1.4° \pm 0.1°$ (Figure 2a) and $0.9° \pm 0.1°$ (Figure 2b). This corrugation angle is determined by bulk crystallographic structure, surface and twinning plane and it is unique for a given combination of the three.

Figure 3 shows the surface topography and the micromagnetic structure of the (110) surface plane. The magnetic domain boundaries are pinned to the twin boundaries, although there is a small number of unpinned boundaries. This behavior can also be observed in Fig. 4 along with various micromagnetic structures on different unspecified surface planes. Angles between domain walls on the (110) surface have well-defined bimodal distribution (Fig. 3c) consistent with cubic magnetocrystalline anisotropy. Simultaneously performed surface potential imaging (SSPM) indicates that the surface potential is uniform within the areas studied as expected on a conductive surface. This indicates the absence of a second phase on surfaces and evidences a purely magnetic origin of MFM images.

Topographic defects (unspecified surface) are associated with an unusual local distortion of micromagnetic structure (Fig. 5). Increased MFM contrast indicates larger out-of-plane magnetization. As confirmed by energy dispersive X-ray analysis, the defect is purely topographical and there is no associated impurity inclusion. Noteworthy is the characteristic labyrinthine magnetization pattern, which is typical for thin films and amorphous materials.

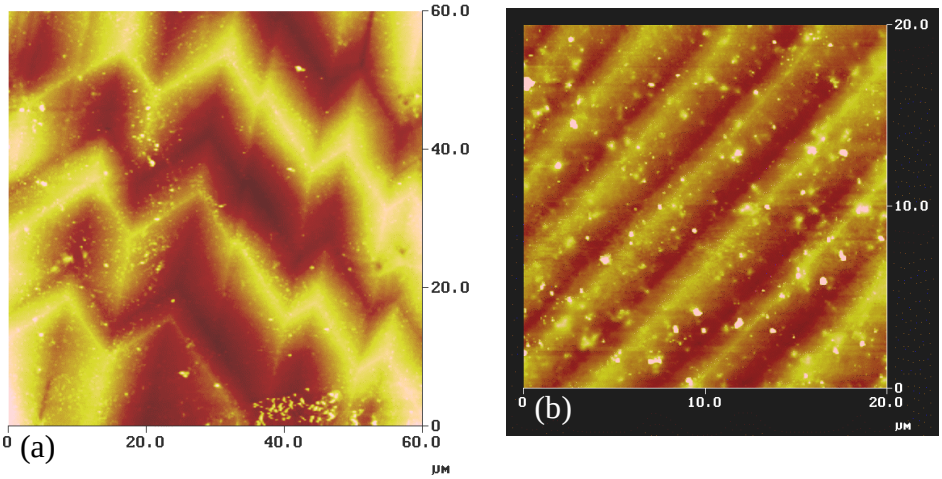

Figure 2. *Surface topography of two regions on as grown LSMO crystals surface.*

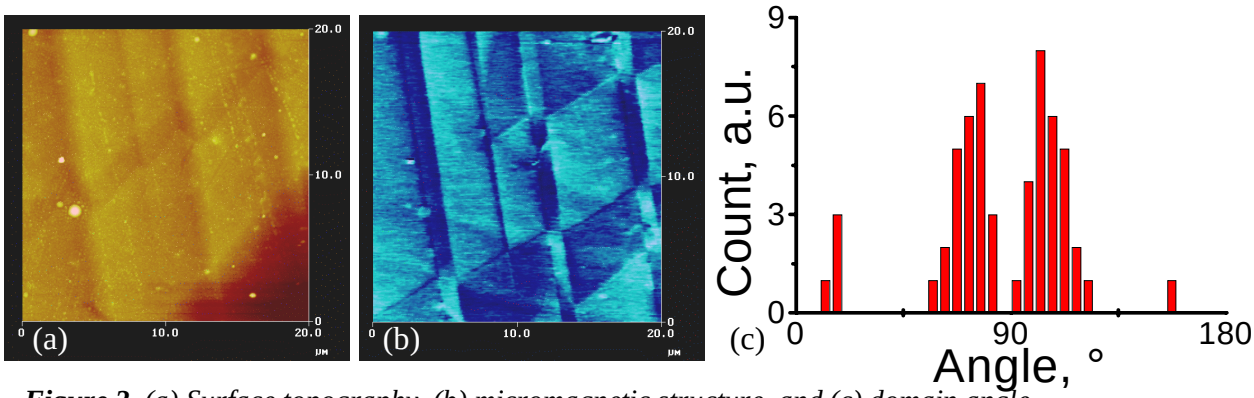

Figure 3. *(a) Surface topography, (b) micromagnetic structure, and (c) domain angle distribution of the (110) surface plane (rhombohedral setting).*

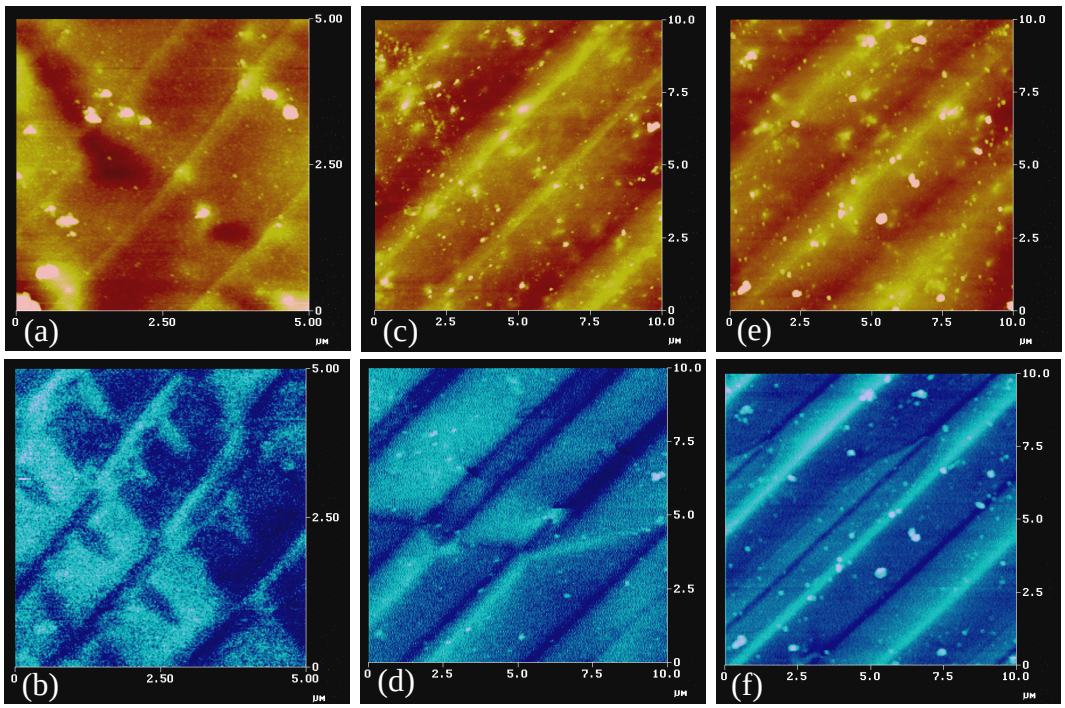

Figure 4. *(a, c, e) Surface topographies and (b, d, f) corresponding micromagnetic structures of various unspecified surface planes.*

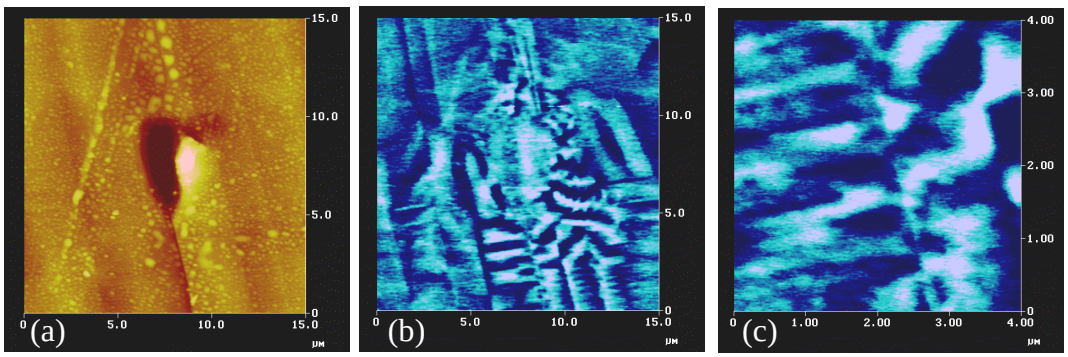

Figure 5. *(a) Surface topography and (b, c) micromagnetic structure of the unspecified surface with a topographic defect on it.*

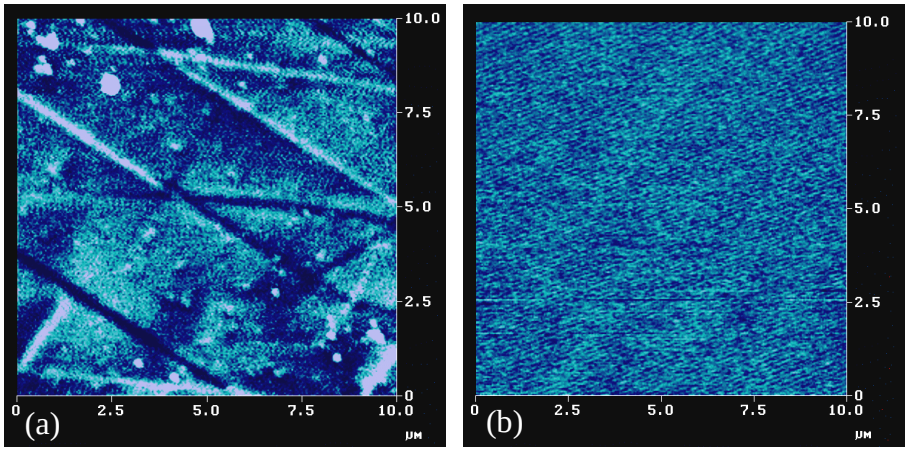

Figure 6. *(a) Micromagnetic structure of the rapidly cooled crystal and (b) micromagnetic structure observed above the Curie temperature.*

Heating the crystal above the Curie temperature and quickly cooling it down to room temperature resulted in a domain structure comprised of 180° Bloch walls with different chiralities (Figure 6a). Heating this crystal again above the Curie temperature resulted in the disappearance of domain structure (Figure 6b) in agreement with theoretical expectations.

ACKNOWLEDGEMENTS

The authors would like to thank Dr. W.H. McCarroll for discussions and help with ICP and Dr. T.J. Emge for single crystal X-ray diffraction measurements.

REFERENCES

1. J.Z. Sun, A. Gupta, *Annual Rev. Mater. Sci.* **28**, 29 (1998) and references therein.
2. W.H. McCarroll, K.V. Ramanujachary, I. Fawcett, and M. Greenblatt, *J. Solid State Chem.* **145**, 88 (1999).
3. M. Déchamps, A.M. de Leon Guevara, L. Pinsard and A. Revcolevschi, *Philosophical Magazine* A **80**(1), 119 (2000).
4. V.A. Cherepanov, L.Yu. Barkhatova, and V.I. Voronin, *J. Solid State Chem.* **134**, 38 (1997).
5. A. Maignan, V. Caignaert, Ch. Simon, M. Hervieu and B. Raveau, *J. Mater. Chem.* **5**(7), 1089 (1995).
6. M.S. Osofsky, B. Nadgorny, R.J. Soulen, Jr., P. Broussard, M. Rubinstein, J. Byers, G. Laprade, Y.M. Mukovskii, D. Shulyatev, and A. Arsenov, *J. Appl. Phys.* **85**, 5567 (1999).
7. N. Abdelmoula, K. Guidara, A. Cheikh-Rouhou, and E. Dhari and J.C. Joubert, *J. Solid State Chem.* **151**, 139 (2000).
8. W.H. McCarroll, K.V. Ramanujachary, M. Greenblatt, and F. Cosandey, *J. Solid State Chem.* **136**, 322 (1998).
9. F. Licci, G. Turilli, P. Ferro, *J. Magn. Magn. Mater.* **164**, L268 (1996).
10. A.C. Larson and R.B. Von Dreele, General Structure Analysis System (GSAS), Los Alamos National Laboratories, Report LAUR 86-748 (1994).
11. J. Töpfer and J.B. Goodenough, *J. Solid State Chem.* **130**, 117 (1997).
12. Scanning Probe Microscopy: Theory, Techniques and Applications, Ed. D.A. Bonnell, Wiley VCH, 2000.